

Article

Cooling Effect and Cooling Speed for a Membrane-in-Middle Optomechanical System

Zhixin Chen ¹, Qing Lin ¹  and Bing He ^{2,*} 

¹ Fujian Key Laboratory of Light Propagation and Transformation, Institute of Systems Science, College of Information Science and Engineering, Huaqiao University, Xiamen 361021, China; zxchen@hqu.edu.cn (Z.C.); qlin@hqu.edu.cn (Q.L.)

² Center for Quantum Optics and Quantum Information, Universidad Mayor, Camino La Pirámide, Huechuraba 5750, Chile

* Correspondence: bing.he@umayor.cl

Abstract: Optomechanical systems are suitable for realizing the ground-state cooling of macroscopic objects. Based on a dynamical approach that goes beyond the validity of the standard linearization approach, we simulate the detailed cooling processes for a membrane-in-middle optomechanical system. In addition to the cooling results, we especially study the cooling speed, which is indicated by how soon the first minimum thermal phonon number is reached. Their relevance to the system parameters provides essential knowledge about how to achieve the best and/or fastest cooling under various combinations of different driving fields.

Keywords: optomechanics; ground-state cooling; dynamical evolution processes

1. Introduction

Rich quantum phenomena will appear when a system is cooled down to an ultra-low temperature. Examples of these phenomena include superconductivity, superfluidity, Bose–Einstein condensation, etc. (see, e.g., [1]). Quantum coherence will be preserved well at low temperatures, since the decoherence due to the thermal noise is highly suppressed [2]. For this purpose, ground-state cooling by various means is regarded as an essential approach to macroscopic quantum states, which can be used to test whether there exists a boundary between the classical and quantum worlds [3,4]. Due to their various advantages, optomechanical systems (OMSs) were considered to be good candidates for realizing such ground-state cooling [5], and a large number of theoretical schemes (see, e.g., [6–16]), as well as several experiments (see, e.g., [17–27]), have been devoted to this field of research in recent years.

An OMS is a nonlinear physical system, and the existence of optomechanical nonlinearity is the core factor for realizing ground-state cooling, macroscopic entanglement generation [28–32], optical frequency combs [33], optical chaos [34], and other physical processes. The quantum properties of an OMS are described by the quantum nonlinear Langevin equations, the solutions of which have not yet been made generally available. The common approach to dealing with such quantum dynamics is a standard linearization procedure by expanding the system operators around the equilibrium states of an evolved system [5,28], which is borrowed from classical nonlinear dynamics. Based on the assumption of such a steady state, the cavity mode is expanded as $\hat{a} \rightarrow \alpha + \delta\hat{a}$, where α is the steady-state value of the cavity mode. Then, the nonlinear equations can be linearized to find the cooling limit $(n_m^f/n_{th}) \times (\Gamma_{opt}/\gamma_m) = 1$ [5], where n_m^f is the final phonon number, n_{th} is the phonon number of the thermal reservoir, Γ_{opt} is the effective optomechanical damping rate related to the cavity's steady-state value, and γ_m is the mechanical damping rate. In fact, steady states should be evolved from an initial state after a period of time. A consideration based on steady states, therefore, cannot provide any information about the evolution process. A different approach based on a dynamical process [15] predicts another



Citation: Chen, Z.; Lin, Q.; He, B. Cooling Effect and Cooling Speed for a Membrane-in-Middle Optomechanical System. *Photonics* **2022**, *9*, 400. <https://doi.org/10.3390/photonics9060400>

Received: 18 May 2022

Accepted: 3 June 2022

Published: 6 June 2022

Publisher's Note: MDPI stays neutral with regard to jurisdictional claims in published maps and institutional affiliations.



Copyright: © 2022 by the authors. Licensee MDPI, Basel, Switzerland. This article is an open access article distributed under the terms and conditions of the Creative Commons Attribution (CC BY) license (<https://creativecommons.org/licenses/by/4.0/>).

optomechanical cooling limit $(n_m^f/n_{th}) \times (\kappa/\gamma_m) = 1$ (κ is the cavity damping rate) and indicates that the cooling result is relevant to cooling speed, which can be measured by the time for reaching the minimum phonon number. Such conclusions were drawn about a single-cavity system driven by a continuous-wave (CW) laser field, for which it was also suggested that, within a wide range of system parameters, a faster cooling process could be beneficial to the cooling result.

The above cooling limit in a single cavity with a CW drive can be generalized to a pulse-driven OMS [35–37] or a membrane-in-middle (MIM) OMS [38,39], where it is more obvious that system steady states in equilibrium do not generally exist. In these situations, the phonon number will not decrease directly to its minimum, but will keep oscillating with time. How their cooling speeds relate to the best cooling results, together with which characteristic quantities depict a cooling process well, have not yet been well understood. The current work fills the gap by studying the real-time cooling processes in MIM systems. To this type of OMS, we apply pulsed drives, CW drives, or their combinations, which necessitate a completely dynamical approach to the corresponding cooling processes. The understanding about ground-state cooling provided here enables the proper choice of system parameters to achieve the best cooling result.

2. Method

An MIM optomechanical system can be built by inserting a thin membrane into an optical cavity of two fixed mirrors, as shown in Figure 1. Its physical properties and application to ground-state cooling were investigated in Refs. [40–47], but the corresponding dynamical evolution processes have not yet been well studied. If the membrane is exactly in the middle, the lengths of the left and right cavities will be the same, and they will have the same resonant cavity frequency, i.e., $\omega_{c1} = \omega_{c2} = \omega_c$. Two driving fields are injected into the left and right cavities, respectively, so that the radiation pressure induces the interaction of the two cavity modes with the mechanical mode. Then, the system Hamiltonian is given as ($\hbar = 1$)

$$\begin{aligned}
 H(t) = & \omega_c \hat{a}_1^\dagger \hat{a}_1 + \omega_c \hat{a}_2^\dagger \hat{a}_2 + \omega_m \hat{b}^\dagger \hat{b} + i \underbrace{\sum_{j=1}^2 [\hat{a}_j^\dagger E_j(t) e^{-i\omega_L t} - \hat{a}_j E_j^*(t) e^{i\omega_L t}]}_{H_L(t)} \\
 & - \underbrace{g_m (\hat{a}_1^\dagger \hat{a}_1 - \hat{a}_2^\dagger \hat{a}_2) (\hat{b} + \hat{b}^\dagger) + J (\hat{a}_2^\dagger \hat{a}_1 + \hat{a}_1^\dagger \hat{a}_2)}_{H_{OM}} \\
 & + i \underbrace{\sum_{j=1}^2 \sqrt{2\kappa_j} [\hat{a}_j^\dagger \hat{\xi}_{c_j}(t) - \hat{a}_j \hat{\xi}_{c_j}^\dagger(t)] + i \sqrt{2\gamma_m} [\hat{b}^\dagger \hat{\xi}_m(t) - \hat{b} \hat{\xi}_m^\dagger(t)]}_{H_{SR}(t)}. \tag{1}
 \end{aligned}$$

where ω_m is the mechanical frequency, $\hat{a}_{1(2)}$ is the cavity field mode, and \hat{b} is the mechanical mode. The drive frequency ω_L of the external drive field can be freely adjusted, and the profile $E(t)$ depends on the drive that we use. The single-photon coupling strength $g_m = X_{ZPL}/L \times \omega_c$ [5] (X_{ZPL} is the zero-point fluctuation amplitude and L is the cavity size) is an important parameter, as it is the strength of the optomechanical interaction in the Hamiltonian H_{OM} . The cavity lengths of the left and right cavities are changed to the opposite directions to have the coupling terms of the two cavity modes with the mechanical mode with the opposite signs. The final part of the stochastic Hamiltonian $H_{SR}(t)$ denotes the coupling of the cavity and mechanical modes to the reservoirs corresponding to the damping rate κ and γ_m , respectively, since the system is an open system here. The cavity and thermal noises are both treated as the white noises, and the corresponding stochastic Langevin noise operators $\hat{\xi}_c, \hat{\xi}_m$ of the reservoirs in thermal equilibrium satisfy [5,48]

$$\langle \hat{\xi}_{c(m)}^\dagger(t) \hat{\xi}_{c(m)}(\tau) \rangle_R = n_{c(m)} \delta(t - \tau), \tag{2}$$

where $n_c = 1/(e^{\hbar\omega_c/k_B T} - 1) \approx 0$, $n_m = 1/(e^{\hbar\omega_m/k_B T} - 1) = n_{th} \gg 1$ (n_m before cooling is equal to n_{th} at a certain temperature). In many other similar systems, the direct coupling of the left and right cavity modes can exist with a strength J , but we assume $J = 0$ (opaque membrane) below. The reason for this choice is that a possible transmission through the membrane can lower the radiation pressure acting on it; obviously, the radiation force on the membrane is highest when the fields are totally reflected from it. It is quantitatively concluded in Ref. [38] that the inter-cavity coupling J should be as small as possible for a cooling process.

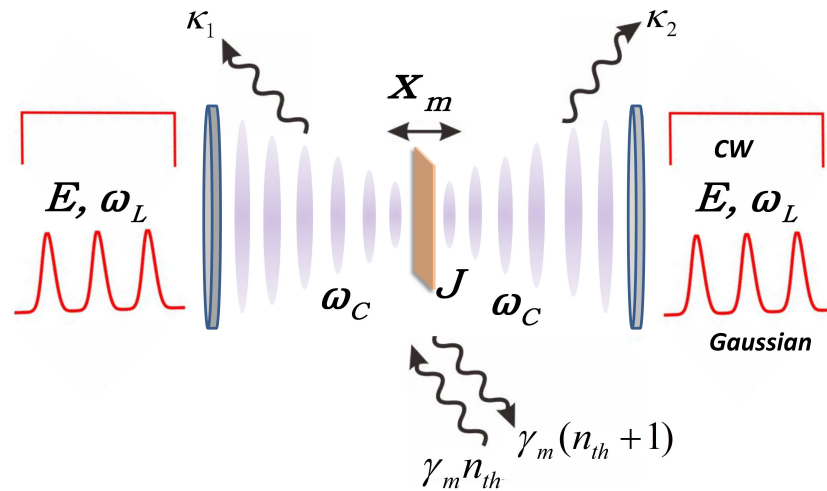


Figure 1. The setup of a membrane-in-middle optomechanical system. A thin membrane is inserted into an optical cavity, and it acts as a mechanical resonator. The system is driven by Gaussian pulses, a continuous-wave field, or both, respectively, on the left and right side, thus creating radiation pressure on the membrane.

One can obtain the dynamical equations of the OMS through the evolution operator $U(t) = \mathcal{T} \exp\{-i \int_0^t d\tau H(\tau)\}$, which is defined as a time-ordered exponential (note that $U(t)$ is not a unitary one due to the stochastic Hamiltonian part) by means of the corresponding Ito rules for the stochastic part of the Hamiltonian [48]. Here, the time-ordered exponential should be used because the Hamiltonian $H(t)$ does not commute at different moments of time t . However, it is almost impossible to find the solutions of the nonlinear dynamical equations directly. The linearization of the system dynamics is beyond the reach of the standard approach based on steady states, especially when the driving fields involve the pulsed ones. In what follows, we apply a method based on the decomposition of the evolution operators [49,50] to deal with the quantum dynamical processes. The first step is to decompose the overall operator $U(t)$ as

$$U(t) = U_1(t)U_2(t) \times \mathcal{T} \exp\{-i \int_0^t d\tau [H_{eff}(\tau) + H_N(\tau)]\}, \tag{3}$$

where

$$\begin{aligned} U_1(t) &= \exp\{-i(\omega_c \hat{a}_1^\dagger \hat{a}_1 + \omega_c \hat{a}_2^\dagger \hat{a}_2 + \omega_m \hat{b}^\dagger \hat{b})t\} \\ U_2(t) &= \exp\{-i \int_0^t d\tau U_1^\dagger(\tau) H_L(\tau) U_1(\tau)\}, \end{aligned} \tag{4}$$

and

$$H_{eff}(t) + H_N(t) = U_2^\dagger(t) U_1^\dagger(t) \{H_{OM}(t) + H_{SR}(t)\} U_1(t) U_2(t). \tag{5}$$

The operators $U_1(t)$ and $U_2(t)$ are reduced to the ordinary exponentials because their corresponding Hamiltonians commute at different times. The specific forms of the

Hamiltonians H_{eff} and H_N can be then found with the following transformations of the cavity modes \hat{a}_1 and \hat{a}_2 and the mechanical mode \hat{b} :

$$\begin{aligned} U_2^\dagger(t)U_1^\dagger(t)\hat{a}_1U_1(t)U_2(t) &= e^{-i\omega_c t}\left(\hat{a}_1 + \int_0^t d\tau E_1(\tau)e^{i\Delta\tau}\right) \equiv e^{-i\omega_c t}(\hat{a}_1 + F_1(t)), \\ U_2^\dagger(t)U_1^\dagger(t)\hat{a}_2U_1(t)U_2(t) &= e^{-i\omega_c t}\left(\hat{a}_2 + \int_0^t d\tau E_2(\tau)e^{i\Delta\tau}\right) \equiv e^{-i\omega_c t}(\hat{a}_2 + F_2(t)), \\ U_2^\dagger(t)U_1^\dagger(t)\hat{b}U_1(t)U_2(t) &= e^{-i\omega_m t}\hat{b}, \end{aligned} \tag{6}$$

with $\Delta = \omega_c - \omega_L$ being the detuning of the drives, while the effective drive profile $F_{1(2)}(t)$ can be transformed from the original drive profile $E_{1(2)}(t)$. This procedure is like a consecutive application of the interaction picture with respect to the free oscillation part and the driving part in Equation (1).

If a CW drive $E(t) = E$ is used, the effective drive profile will be

$$F(t) = \frac{iE}{\Delta}(1 - e^{i\Delta t}). \tag{7}$$

On the other hand, when a Gaussian pulse drive $E(t) = \sum_n E \exp^{-(t-nt_0)^2/\sigma^2}$ ($n = 1, 2, \dots$) is applied, the effective drive profile will take the form

$$\begin{aligned} F(t) &= \sum_n \int_0^t d\tau E \exp\left\{-\frac{(\tau - nt_0)^2}{\sigma^2}\right\} e^{i\Delta\tau} \\ &= \sum_n \frac{i\sqrt{\pi}\sigma E}{2} \exp\left\{i\Delta \cdot nt_0 - \frac{\Delta^2\sigma^2}{4}\right\} \text{Erfi}\left[\frac{-2i(t - nt_0) - \Delta \cdot \sigma^2}{2\sigma}\right], \end{aligned} \tag{8}$$

where t_0 is the center moment of the Gaussian pulse, 2σ is the pulse width, and $\text{Erfi}(z) = -i\text{Erf}(iz)$ is the imaginary error function. From the transformations in Equation (6), one will have the following:

$$\begin{aligned} H_{eff}(t) &= -g_m \left\{ \left[F_1(t)\hat{a}_1^\dagger + F_1^*(t)\hat{a}_1 + |F_1(t)|^2 \right] - \left[F_2(t)\hat{a}_2^\dagger + F_2^*(t)\hat{a}_2 + |F_2(t)|^2 \right] \right\} \\ &\quad \times (e^{-i\omega_m t}\hat{b} + e^{i\omega_m t}\hat{b}^\dagger) + i \sum_{j=1}^2 \sqrt{2\kappa_j} \left\{ e^{i\omega_c t} (\hat{a}_j^\dagger + F_j^*(t)) \hat{\xi}_{c_j}(t) - H.c. \right\} \\ &\quad + i\sqrt{2\gamma_m} (e^{i\omega_m t}\hat{b}^\dagger \hat{\xi}_m(t) - H.c.), \\ H_N(t) &= -g_m (\hat{a}_1^\dagger \hat{a}_1 - \hat{a}_2^\dagger \hat{a}_2) (e^{-i\omega_m t}\hat{b} + e^{i\omega_m t}\hat{b}^\dagger) \end{aligned} \tag{9}$$

transformed from the original Hamiltonian.

The effective Hamiltonian H_{eff} explicitly displays the beam-splitter (BS) action and squeezing (SQ) action with the terms that it contains

$$\begin{aligned} -g_m \frac{iE}{\Delta} (1 - e^{i\Delta t}) e^{-i\omega_m t} \hat{b} \hat{a}_1^\dagger + g_m \frac{iE}{\Delta} (1 - e^{i\Delta t}) e^{-i\omega_m t} \hat{b} \hat{a}_2^\dagger + H.c. &\equiv H_{BS}, \\ -g_m \frac{iE}{\Delta} (1 - e^{i\Delta t}) e^{i\omega_m t} \hat{b}^\dagger \hat{a}_1^\dagger + g_m \frac{iE}{\Delta} (1 - e^{i\Delta t}) e^{i\omega_m t} \hat{b}^\dagger \hat{a}_2^\dagger + H.c. &\equiv H_{SQ} \end{aligned} \tag{10}$$

(here, we simply consider the situation of two identical CW drives for clarity). The BS Hamiltonian acts as a conversion between the cavity modes and mechanical mode, so that the mechanical oscillation is transferred to the cavity fields coupled to a cold reservoir, realizing the cooling of the mechanical oscillator. The SQ Hamiltonian, however, acts like a magnifier to increase the cavity and mechanical occupations together, having the effect of raising the the equivalent temperature of the mechanical oscillator. If $\Delta = \omega_m$, one oscillating phase factor in H_{BS} will be canceled so that the BS action is enhanced to have a coefficient $J_E = g_m/\omega_m \times E/\kappa_1$ without being accompanied by the oscillating phase factor that suppresses the BS effect. This coefficient is called the effective coupling intensity [15],

and it appears in both H_{BS} and H_{SQ} with a difference in whether it is with oscillating phase factors or not. On the other hand, the Hamiltonian $H_N(t)$ is still a nonlinear one, but it does not contain the effective drive $F(t)$. Under the conditions $g_m/\omega_m \ll 1$ (here, $g_m/\omega_m = 10^{-7}$), the effect of $H_N(t)$ can be safely neglected [32]. Moreover, the addition of the phase terms and the displacements for the system operators due to the combined action of $U_1(t)$ and $U_2(t)$ do not change the properties of the stochastic Hamiltonian H_{SR} with the redefinition of the noise operators [32]. Therefore, the effective Hamiltonian $H_{eff}(t)$ leads to the following linearized dynamical equations:

$$\begin{aligned} \dot{\hat{a}}_1 &= -\kappa_1 \hat{a}_1 + ig_m F_1(t) (e^{-i\omega_m t} \hat{b} + e^{i\omega_m t} \hat{b}^\dagger) - \kappa_1 F_1(t) + \sqrt{2\kappa_1} e^{i\omega_c t} \hat{\xi}_{c_1}(t), \\ \dot{\hat{b}} &= -\gamma_m \hat{b} + ig_m e^{i\omega_m t} [F_1(t) \hat{a}_1^\dagger + F_1^*(t) \hat{a}_1 - F_2(t) \hat{a}_2^\dagger - F_2^*(t) \hat{a}_2] \\ &\quad + ig_m e^{i\omega_m t} (|F_1(t)|^2 - |F_2(t)|^2) + \sqrt{2\gamma_m} e^{i\omega_m t} \hat{\xi}_m(t), \\ \dot{\hat{a}}_2 &= -\kappa_2 \hat{a}_2 - ig_m F_2(t) (e^{-i\omega_m t} \hat{b} + e^{i\omega_m t} \hat{b}^\dagger) - \kappa_2 F_2(t) + \sqrt{2\kappa_2} e^{i\omega_c t} \hat{\xi}_{c_2}(t), \end{aligned} \quad (11)$$

which determine a cooling process.

3. Results

Applying the dynamical equations in Equation (11), we will simulate various cooling processes and clarify the relevance of the cooling results and cooling speeds with the system parameters. A cooling process is illustrated by the dynamical evolution the thermal phonon number $n_m(t) = \langle \hat{b}^\dagger(t) \hat{b}(t) \rangle - \langle \hat{b}^\dagger(t) \rangle \langle \hat{b}(t) \rangle$ from the numerical solutions of Equation (11). One needs to see how fast $n_m(t)$ reaches the minimums and how these minimums could be. Here, all system parameters in the numerical simulations are scaled with respect to the damping rate κ_1 so that we only deal with their dimensionless quantities.

3.1. Dynamical Evolution of the Thermal Phonon Number

To analyze the relations between the cooling result and cooling speed, we first simulate some dynamical evolution processes of the thermal phonon number under different combinations of drives, which are illustrated in Figure 2. Here, the effective drive intensity is set to be $J_E = 0.5, 1, 2, 4$. In Figure 2a, two Gaussian pulsed drives with the same pulse width $\sigma = 3/\kappa_1$ and peak time $t_0 = 2\sigma$ are applied to the left and right cavity, respectively. By setting the starting time of the right drive $t_s = 2\sigma$, the large portions of the fields created by these two pulsed drives act on the membrane in turn, and then a better cooling effect can be achieved as compared to the other time lags between the peaks of the two pulsed drives. The phonon number will thus be decreased to less than 1, which can be regarded as the mechanical resonator being cooled to its ground state. It is evident that a cooling process speeds up with the increase in effective drive intensity J_E , together with the decrease in the minimum achievable phonon number. For example, the first minimum achievable phonon number is $n_m^1 = 0.139$ for $J_E = 2$ (pink line), which is associated with the evolution time $\kappa_1 t_1 = 4.530$; for $J_E = 4$ (black line), the first minimum achievable phonon number is slightly decreased to be $n_m^1 = 0.111$, and the evolution time is decreased to $\kappa_1 t_1 = 3.444$. On the other hand, in Figure 2a, after evolving for the time $\kappa_1 t_f = 12.281$, the phonon number under $J_E = 2$ reaches the final minimum $n_m^f = 0.1017$, while for $J_E = 4$, the evolution time for reaching this minimum phonon number is slightly decreased to $\kappa_1 t_f = 12.124$, and the final achievable minimum phonon number decreases to $n_m^f = 0.0511$, corresponding to a ratio of $(n_m^f/n_{th}) \times (\kappa_1/\gamma_m) = 0.511$, which has surpassed the theoretical cooling limit $(n_m^f/n_{th}) \times (\kappa_1/\gamma_m) = 1$ for a single CW drive acting on a single cavity [15]. Moreover, from this comparison, one sees that the pulsed drives can sometimes outdo the CW ones in the cooling processes.

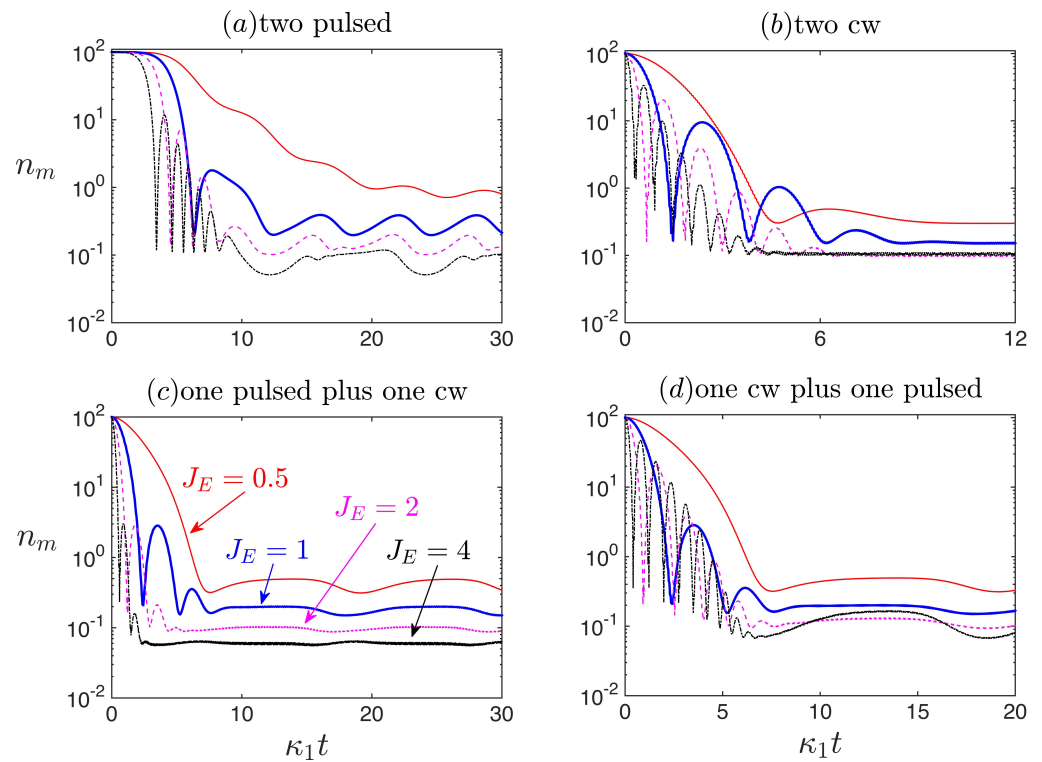


Figure 2. Dynamical evolution processes of the thermal phonon number under different combinations of a Gaussian pulsed drive and CW drive. Each cavity is driven by one drive, and the effective coupling intensity is $J_E = 0.5, 1, 2, 4$ for red, blue, pink, and black lines, respectively. For a pulsed field, the parameter J_E is determined by its peak amplitude E . (a) Both drives are Gaussian pulsed. (b) Both drives are CW ones. (c) One Gaussian pulsed drive and one CW drive are applied to the left and right cavity, respectively. (d) The pulsed one and CW one in (c) are interchanged in their positions. The re-scaled optomechanical coupling constant is $g_m/\kappa_1 = 10^{-5}$; the re-scaled mechanical frequency is $\omega_m/\kappa_1 = 100$; the re-scaled mechanical damping rate is $\gamma_m/\kappa_1 = 10^{-3}$; the initial thermal occupation is $n_{th} = 100$. The ratio of the damping rates of the two cavities is $\kappa_2/\kappa_1 = 1$ for $J_E = 0.5$ and $\kappa_2/\kappa_1 = J_E$ for $J_E = 1, 2, 4$, so that most results in (c) are not the same as those in (d).

The overall tendencies are similar in Figure 2c,d. However, there exists one difference from the pattern in Figure 2b. The evolution time for reaching the first minimum phonon number due to $J_E = 4$ is shorter than the time due to $J_E = 2$, since the cooling is faster with a higher effective drive intensity, but the final minimum phonon number under the condition $J_E = 4$ is about $n_m^f = 0.1005$, which becomes slightly larger than the one at $n_m^f = 0.0961$ under the condition $J_E = 2$. Therefore, the cooling result and cooling speed do not always match one another. For example, the cooling speed with the condition $J_E = 4$ is higher, but the corresponding first minimum phonon number is only $n_m^1 = 1.3458$, as compared with $n_m^1 = 0.1581$ under $J_E = 2$, which is a difference of almost one order in this first minimum phonon number.

The illustrated cooling results and cooling speeds reflect the competition of the co-existing BS effect and SQ effect. Even when the system works at the resonant point of red detuning at $\Delta = \omega_m$, the SQ effect of heating the mechanical resonator still acts at a certain rate, though the BS effect dominates in this situation. Under the competition between the two effects, the phonon number does not decrease directly to the minimum, but oscillates with time. When the BS effect dominates, the resonator can be quickly cooled down to the first minimum n_m^1 , but, as the heating effect accumulates slowly, the phonon number will rebound from time to time, and an oscillating phonon number manifests. Only after the competition between the two effects becomes completely balanced can the phonon number reach its minimum. When the effective coupling intensity is not so large, the BS effect is enhanced faster than the SQ effect, but the SQ effect grows faster when the effective coupling intensity J_E becomes sufficiently large. Especially when the effective coupling

intensity is increased from $J_E = 2$ to $J_E = 4$, as shown in Figure 2b, the first minimum phonon number increases from $n_m^1 = 0.1581$ to $n_m^1 = 1.3458$ by almost one order. This clearly indicates a stronger SQ effect, which raises the final minimum photon number when the coupling J_E becomes even higher. In a sense, the illustrated cooling result and cooling speed in a process directly measure the inherent BS and SQ effects under a certain condition for OMSs.

3.2. Determination of the Cooling Result and Cooling Speed

From the illustrated dynamical evolution processes, we see that the first minimum phonon number n_m^1 , its corresponding evolution time $\kappa_1 t_1$, and the final minimum phonon number n_m^f constitute the three characteristic quantities for depicting a cooling process. The relations between these figures of merit and the effective coupling intensity J_E are illustrated in Figures 3 and 4, respectively, for the systems driven by two pulsed drives or one pulsed plus one CW drive. In both scenarios, the evolution time $\kappa_1 t_1$ to the first minimum n_m^1 drops with the increased effective coupling intensity, simply due to an enhanced BS effect during the initial transient period of a cooling process. However, the reduction of the evolution time becomes less and less significant as the effective coupling J_E is increased further. It will show a saturation at large values of J_E , where the SQ effect grows more quickly.

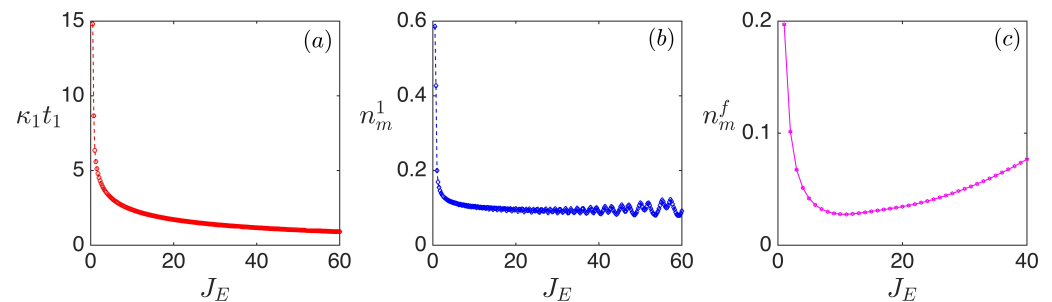


Figure 3. Relations between the three figures of merit with the effective coupling intensity J_E in the scenario of two pulsed drives. (a) The evolution time for reaching the first minimum phonon number vs. the effective coupling intensity. (b) The first minimum phonon number vs. the effective drive intensity. There exists oscillation if $J_E > 10$. (c) The final minimum phonon number vs. the effective coupling intensity. The quantity increases when $J_E > 10$. The fixed system parameters are the same as those in Figure 2.

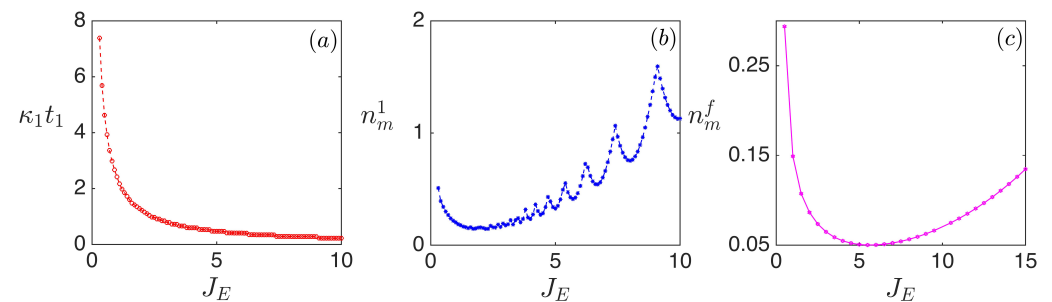


Figure 4. Corresponding relations between the three figures of merit with the effective coupling intensity J_E in the scenario of one pulsed drive to the left cavity plus one CW drive to the right cavity.

Initially, with the increased effective coupling intensity J_E , the corresponding first minimum phonon number n_m^1 decreases quickly, but the decreasing tendency also becomes less and less significant when $J_E > 2$. This tendency of this figure of merit reflects the fact that the SQ effect is obviously enhanced. The condition $J_E > 2$ can be, therefore, seen as the beginning of having a considerable SQ effect. An obvious periodic tail in Figure 4b manifests the competition between the BS and SQ effect well. Such a drastic oscillation of n_m^1 to large amplitudes exists in the scenario involving CW drives, indicating that the SQ effect is more significant in this scenario. Here, the CW drive acts continuously in

contrast to the pulsed ones with gaps of non-action during the cooling process. Because the SQ action takes a continuous period of time to accumulate its effect, this continuous process can be interrupted in the scenario of pulsed drives so that it is possible to reduce the harmful SQ effect by setting the appropriate intervals for a pulsed drive. This is why the theoretical cooling limit for a single cavity driven by a single CW drive can be surpassed by pulsed drives [35–37].

When the effective coupling intensity is within the range $J_E < 10$ in Figure 3c or $J_E < 6$ in Figure 4c, the final minimum phonon number n_m^f (the cooling result) is lowered together with the evolution time $\kappa_1 t_1$ to the first minimum. However, once the effect of coupling intensity becomes even larger, the quantity n_m^f will go up together with n_m^1 due to the more enhanced SQ effect. Compared with the pulsed scenario, setups involving a CW drive can achieve their best cooling results with the lower J_E , since the action of the CW drive is continuous. The correspondingly lower pumping power required for cooling is an advantage for the scenario with CW drive. For the final cooling result n_m^f , its increase with the effective coupling J_E is always faster in the scenario involving one CW drive due to the more significant SQ effect.

The relations between the three figures of merit, n_m^1 , $\kappa_1 t_1$, and n_m^f , and the effective coupling intensity J_E are not so trivial, as shown in Figures 3 and 4. Faster cooling does not necessarily imply better a cooling result. Usually, an effective coupling intensity leading to a relatively fast cooling together with a low first minimum phonon number n_m^1 is a good choice for achieving satisfactory cooling results. In reality, one should set the proper J_E when designing experiments while considering the existing conditions for the specific setups.

3.3. Effect of the Mechanical Damping Rate

In the above discussion, the mechanical frequency and damping rate are fixed as $\omega_m/\kappa = 100$ and $\gamma_m/\kappa = 10^{-3}$, respectively, to be in the resolved sideband regime. As pointed out in the former works [15,38], under a fixed J_E , a larger mechanical frequency is beneficial for achieving a better cooling result, since the coexisting SQ effect can be suppressed in this way. The second factor is the damping rate, which obviously improves the cooling result when it is lowered. How this factor affects the cooling result and cooling speed is another interesting issue. To clarify this point, we display the dynamical evolution of the phonon number with different damping rates $\gamma_m/\kappa_1 = 10^{-1}, 10^{-2}, 10^{-3}, 10^{-4}$ under the effective coupling intensities $J_E = 2, 4, 10, 20$, respectively, in Figure 5. The evolution processes show that the cooling speeds are almost the same for all different damping rates, but the corresponding first minimum phonon numbers decrease with γ_m . For the effective coupling intensities in Figure 5a,b, the ratios $(n_m^1/n_{th}) \times (\kappa_1/\gamma_m)$ and $(n_m^f/n_{th}) \times (\kappa_1/\gamma_m)$ are preserved to be the same; n_m^1 and n_m^f are simply proportional to the mechanical damping rate, so that one will get a better cooling result by decreasing the damping rate.

When the effective coupling intensity becomes larger, as in Figure 5c,d, the ratios $(n_m^1/n_{th}) \times (\kappa_1/\gamma_m)$ and $(n_m^f/n_{th}) \times (\kappa_1/\gamma_m)$ will no longer be preserved. For example, the first minimum phonon number is $n_m^1 = 0.1031$ for $\gamma_m/\kappa_1 = 10^{-3}$, while $n_m^1 = 0.0149$ for $\gamma_m/\kappa_1 = 10^{-4}$, so that the corresponding ratio $(n_m^1/n_{th}) \times (\kappa_1/\gamma_m)$ changes from 1.031 to 1.49. The cooling effect is obviously impaired, as compared to the situations with relative low effective coupling intensity. Exactly the SQ effect for heating the mechanical resonator will be enhanced with a larger effective coupling intensity J_E , making it harder to improve the cooling simply by increasing the mechanical quality factor.

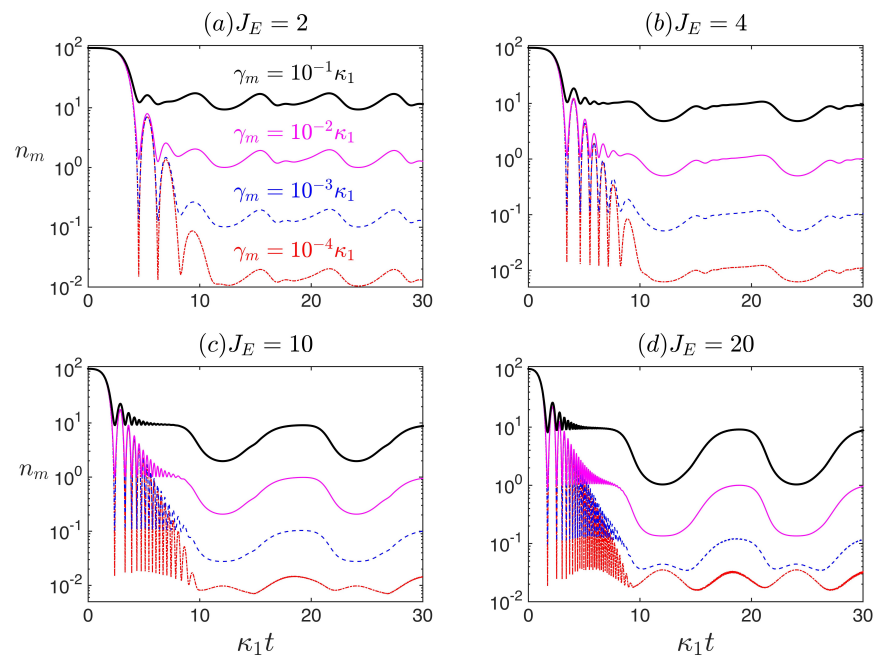


Figure 5. Dynamical evolution processes under two pulsed drives, which are simulated for various damping rates γ_m while the effective coupling intensity is fixed (four different values of $J_E = 2, 4, 10,$ and 20 are considered, respectively). Here, $\gamma_m/\kappa_1 = 10^{-1}$ (black), 10^{-2} (pink), 10^{-3} (blue), and 10^{-4} (red), respectively. The fixed parameters are the same as those in Figure 2.

4. Discussion

The results illustrated above actually reflect how the system parameters, including the drive amplitude E , the single-photon coupling strength g_m , the mechanical frequency ω_m , the damping rate γ_m , and κ_1 and κ_2 are relevant to a cooling process. This relevance can be simply reduced to a single parameter, the effective coupling intensity $J_E = g_m/\omega_m \times E/\kappa_1$. Although increasing the cooling rate with J_E is beneficial to cooling in a certain regime, the SQ effect that heats the system will be enhanced at the same time with J_E . How to balance the BS and SQ effect with an effective coupling intensity is always a central issue in achieving the optimal cooling. The difference in two drive intensities can also affect the cooling result, but it will not lead to a qualitative change, so we set the drive intensity of the two drives to be equal ($E_1 = E_2 = E$) in the illustrations. It should be noted that the ratio κ_2/κ_1 of the damping rates for the two cavities is another relevant factor. The best choice of the ratio is to let it be approximately equal to the effective drive intensity J_E [38]. In most of the above illustrations, we adopt this ratio to show the capacity of the concerned setups. Certainly, the realistic setups without such specific choices qualitatively demonstrate similar behaviors.

5. Conclusions

We applied a dynamical approach in order to study cooling processes with a type of OMS. The dynamical approach not only enables one to find the cooling limit, but also allows one to see how fast a cooling process can be. A cooling process can be well depicted by three figures of merit: n_m^1 , $\kappa_1 t_1$, and n_m^f , and their relations to the effective coupling intensity J_E reflect the existing BS and SQ effects in a specific process. Generally, the accumulated SQ effect takes a longer time to manifest in the cooling process, so it will affect the final cooling result n_m^f more significantly. The BS effect, on the other hand, solely controls the time $\kappa_1 t_1$ to reach the first minimum phonon number n_m^1 , which is also determined by the SQ effect, especially when the effective coupling intensity is very high. Due to the competition of these two effects, it is not ideal to implement a cooling with a large J_E . An optimal cooling occurs under a suitable combination of the effective coupling intensity and mechanical

quality factor. The knowledge obtained here may help to design experiments relevant to optomechanical cooling.

Author Contributions: Calculation, Z.C.; original draft preparation, Q.L.; writing and revision, B.H. All authors have read and agreed to the published version of the manuscript.

Funding: This research was funded by the Natural Science Foundation of China (Grant No. 11574093) and the Natural Science Foundation of Fujian Province of China (NSFFPC) (2020J01061).

Institutional Review Board Statement: Not applicable.

Informed Consent Statement: Not applicable.

Data Availability Statement: Not applicable.

Conflicts of Interest: The authors declare no conflict of interest.

References

1. Coleman, P. *Introduction to Many-Body Physics*; Cambridge University Press: Cambridge, UK, 2015.
2. Zurek, W.H. Decoherence, einselection, and the quantum origins of the classical. *Rev. Mod. Phys.* **2003**, *75*, 715–775. [[CrossRef](#)]
3. Leggett, A.J.; Garg, A. Quantum mechanics versus macroscopic realism: Is the flux there when nobody looks? *Phys. Rev. Lett.* **1985**, *54*, 857–860. [[CrossRef](#)]
4. Leggett, A.J. Testing the limits of quantum mechanics: Motivation, state of play, prospects. *J. Phys. Cond. Mat.* **2002**, *14*, R415–R451. [[CrossRef](#)]
5. Aspelmeyer, M.; Kippenberg, T.J.; Marquardt, F. Cavity optomechanics. *Rev. Mod. Phys.* **2014**, *86*, 1391–1452. [[CrossRef](#)]
6. Wilson-Rae, I.; Nooshi, N.; Zwerger, W.; Kippenberg, T.J. Theory of ground state cooling of a mechanical oscillator using dynamical backaction. *Phys. Rev. Lett.* **2007**, *99*, 093901. [[CrossRef](#)] [[PubMed](#)]
7. Marquardt, F.; Chen, J.P.; Clerk, A.A.; Girvin, S.M. Quantum theory of cavity-assisted sideband cooling of mechanical motion. *Phys. Rev. Lett.* **2007**, *99*, 093902. [[CrossRef](#)]
8. Marquardt, F.; Clerk, A.A.; Girvin, S.M. Quantum theory of optomechanical cooling. *J. Mod. Opt.* **2008**, *55*, 3329–3338. [[CrossRef](#)]
9. Genes, C.; Vitali, D.; Tombesi, P.; Gigan, S.; Aspelmeyer, M. Ground-state cooling of a micromechanical oscillator: Comparing cold damping and cavity-assisted cooling schemes. *Phys. Rev. A* **2008**, *77*, 033804. [[CrossRef](#)]
10. Dantan, A.; Genes, C.; Vitali, D.; Pinard, M. Self-cooling of a movable mirror to the ground state using radiation pressure. *Phys. Rev. A* **2008**, *77*, 011804. [[CrossRef](#)]
11. Li, Y.; Wu, L.A.; Wang, Y.D.; Yang, L.P. Nondeterministic ultrafast ground-state cooling of a mechanical resonator. *Phys. Rev. B* **2011**, *84*, 094502. [[CrossRef](#)]
12. Wang, X.T.; Vinjanampathy, S.; Strauch, F.W.; Jacobs, K. Ultraefficient cooling of resonators: Beating sideband cooling with quantum control. *Phys. Rev. Lett.* **2011**, *107*, 177204. [[CrossRef](#)] [[PubMed](#)]
13. Liu, Y.C.; Xiao, Y.-F.; Luan, X.; Wong, C.W. Dynamic dissipative cooling of a mechanical resonator in strong coupling optomechanics. *Phys. Rev. Lett.* **2013**, *110*, 153606. [[CrossRef](#)]
14. Liu, Y.C.; Hu, Y.W.; Wong, C.W.; Xiao, Y.F. Review of cavity optomechanical cooling. *Chin. Phys. B* **2013**, *22*, 114213. [[CrossRef](#)]
15. He, B.; Yang, L.; Lin, Q.; Xiao, M. Radiation pressure cooling as a quantum dynamical process. *Phys. Rev. Lett.* **2017**, *118*, 233604. [[CrossRef](#)]
16. Lai, D.G.; Huang, J.F.; Yin, X.L.; Hou, B.P.; Li, W.; Vitali, D.; Nori, F.; Liao, J.Q. Nonreciprocal ground-state cooling of multiple mechanical resonators. *Phys. Rev. A* **2020**, *102*, 011502. [[CrossRef](#)]
17. Teufel, J.D.; Harlow, J.W.; Regal, C.A.; Lehnert, K.W. Dynamical backaction of microwave fields on a nanomechanical oscillator. *Phys. Rev. Lett.* **2008**, *101*, 197203. [[CrossRef](#)]
18. Gröblacher, S.; Hertzberg, J.B.; Vanner, M.R.; Gigan, S.; Schwab, K.C.; Aspelmeyer, M. Demonstration of an ultracold micro-optomechanical oscillator in a cryogenic cavity. *Nat. Phys.* **2009**, *5*, 485–488. [[CrossRef](#)]
19. Schliesser, A.; Arcizet, O.; Rivi re, R.; Anetsberger, G.; Kippenberg, T.J. Resolved-sideband cooling and position measurement of a micromechanical oscillator close to the Heisenberg uncertainty limit. *Nat. Phys.* **2009**, *5*, 509–514. [[CrossRef](#)]
20. Park, Y.-S.; Wang, H. Resolved-sideband and cryogenic cooling of an optomechanical resonator. *Nat. Phys.* **2009**, *5*, 489–493. [[CrossRef](#)]
21. O’Connell, A.D.; Hofheinz, M.; Ansmann, M.; Bialczak, R.C.; Lenander, M.; Lucero, E.; Neeley, M.; Sank, D.; Wang, H.; Weides, M.; et al. Quantum ground state and single-phonon control of a mechanical resonator. *Nature* **2010**, *464*, 697–703. [[CrossRef](#)] [[PubMed](#)]
22. Rocheleau, T.; Ndukum, T.; Macklin, C.; Hertzberg, J.B.; Clerk, A.A.; Schwab, K.C. Preparation and detection of a mechanical resonator near the ground state of motion. *Nature* **2010**, *463*, 72–75. [[CrossRef](#)]
23. Teufel, J.D.; Donner, T.; Li, D.; Harlow, J.H.; Allman, M.S.; Cicak, K.; Sirois, A.J.; Whittaker, J.D.; Lehnert, K.W.; Simmonds, R.W. Sideband cooling of micromechanical motion to the quantum ground state. *Nature* **2011**, *475*, 359–363. [[CrossRef](#)]
24. Chan, J.; Alegre, T.P.M.; Safavi-Naeini, A.H.; Hill, J.T.; Krause, A.; Gröblacher, S.; Aspelmeyer, M.; Painter, O. Laser cooling of a nanomechanical oscillator into its quantum ground state. *Nature* **2011**, *478*, 89–92. [[CrossRef](#)]

25. Verhagen, E.; Deléglise, S.; Weis, S.; Schliesser, A.; Kippenberg, T.J. Quantum-coherent coupling of a mechanical oscillator to an optical cavity mode. *Nature* **2012**, *482*, 63–67. [[CrossRef](#)] [[PubMed](#)]
26. Peterson, R.W.; Purdy, T.P.; Kampel, N.S.; Andrews, R.W.; Yu, P.-L.; Lehnert, K.W.; Regal, C.A. Laser cooling of a micromechanical membrane to the quantum backaction limit. *Phys. Rev. Lett.* **2016**, *116*, 063601. [[CrossRef](#)]
27. Clark, J.B.; Lecocq, F.; Simmonds, R.W.; Aumentado, J.; Teufel, J.D. Sideband cooling beyond the quantum backaction limit with squeezed light. *Nature* **2017**, *541*, 191–195. [[CrossRef](#)]
28. Vitali, D.; Gigan, S.; Ferreira, A.; Böhm, H.R.; Tombesi, P.; Guerreiro, A.; Vedral, V.; Zeilinger, A.; Aspelmeyer, M. Optomechanical Entanglement between a Movable Mirror and a Cavity Field. *Phys. Rev. Lett.* **2007**, *98*, 030405. [[CrossRef](#)] [[PubMed](#)]
29. Palomaki, T.A.; Teufel, J.D.; Simmonds, R.W.; Lehnert, K.W. Entangling mechanical motion with microwave fields. *Science* **2013**, *342*, 710–713. [[CrossRef](#)]
30. Lin, Q.; He, B. Optomechanical entanglement under pulse drive. *Opt. Express* **2015**, *23*, 24497. [[CrossRef](#)]
31. Chen, Z.X.; Lin, Q.; He, B.; Lin, Z.Y. Entanglement dynamics in double-cavity optomechanical systems. *Opt. Express* **2017**, *25*, 17237. [[CrossRef](#)]
32. Lin, Q.; He, B.; Xiao, M. Entangling two macroscopic mechanical resonators at high temperature. *Phys. Rev. Appl.* **2020**, *13*, 034030. [[CrossRef](#)]
33. Kippenberg, T.J.; Holzwarth, R.; Diddams, S.A. Microresonator-Based Optical Frequency Combs. *Science* **2011**, *332*, 555–559. [[CrossRef](#)]
34. Jiang, X.F.; Shao, L.B.; Zhang, S.X.; Yi, X.; Wiersig, J.; Wang, L.; Gong, Q.H.; Lonar, M.; Yang, L.; Xiao, Y.F. Chaos-assisted broadband momentum transformation in optical microresonators. *Science* **2017**, *358*, 344–347. [[CrossRef](#)]
35. Lin, Q.; He, B. Highly efficient cooling of mechanical resonator with square pulse drives. *Opt. Express* **2018**, *26*, 33830. [[CrossRef](#)] [[PubMed](#)]
36. Chen, Z.X.; Lin, Q. Cooling the mechanical resonator by Gaussian pulses. *Sci. Sin-Phys. Mech. Astron.* **2020**, *50*, 034213. (In Chinese)
37. Chen, Z.X.; He, B.; Lin, Q. Efficient ground state cooling of a membrane by the combination of continuous-wave field and pulses. *J. Phys. B-Atom. Mol. Opt. Phys.* **2021**, *54*, 095502. [[CrossRef](#)]
38. Wang, C.; Lin, Q.; He, B. Breaking the optomechanical cooling limit by two drive fields on a membrane-in-the-middle system. *Phys. Rev. A* **2019**, *99*, 023829. [[CrossRef](#)]
39. Zhai Y.; Chen, Z.X.; Lin, Q. Efficient ground state cooling of a mechanical resonator in a membrane-in-the-middle system by a single drive. *J. Phys. B-Atom. Mol. Opt. Phys.* **2020**, *37*, 956–962. [[CrossRef](#)]
40. Meystre, P.; Wright, E.M.; McCullen, J.D.; Vignes, E. Theory of radiation-pressure-driven interferometers. *J. Opt. Soc. Am. B* **1985**, *2*, 1830–1840. [[CrossRef](#)]
41. Bhattacharya, M.; Meystre, P. Trapping and cooling a mirror to its quantum mechanical ground state. *Phys. Rev. Lett.* **2007**, *99*, 073601. [[CrossRef](#)] [[PubMed](#)]
42. Jayich, A.M.; Sankey, J.C.; Zwickl, B.M.; Yang, C.; Thompson, J.D.; Girvin, S.M.; Clerk, A.A.; Marquardt, F.; Harris, J.G.E. Dispersive optomechanics: A membrane inside a cavity. *New J. Phys.* **2008**, *10*, 095008. [[CrossRef](#)]
43. Li, Y.; Wu, L.A.; Wang, Z.D. Fast ground-state cooling of mechanical resonators with time-dependent optical cavities. *Phys. Rev. A* **2011**, *83*, 043804. [[CrossRef](#)]
44. Karuza, M.; Molinelli, C.; Galassi, M.; Biancofiore, C.; Natali, R.; Tombesi, P.; Di Giuseppe, G.; Vitali, D. Optomechanical sideband cooling of a thin membrane within a cavity. *New J. Phys.* **2012**, *14*, 095015. [[CrossRef](#)]
45. Guo, Y.J.; Li, K.; Nie, W.J.; Li, Y. Electromagnetically-induced-transparency-like ground-state cooling in a double-cavity optomechanical system. *Phys. Rev. A* **2014**, *90*, 053841. [[CrossRef](#)]
46. Liu, Y.C.; Xiao, Y.F.; Luan, X.S.; Gong, Q.H.; Wong, C.W. Coupled cavities for motional ground-state cooling and strong optomechanical coupling. *Phys. Rev. A* **2015**, *91*, 033818. [[CrossRef](#)]
47. Piergentili, P.; Catalini, L.; Bawaj, M.; Zippilli, S.; Malossi, N.; Natali, R.; Vitali, D.; Di Giuseppe, G. Two-membrane cavity optomechanics. *New J. Phys.* **2018**, *20*, 083024. [[CrossRef](#)]
48. Gardiner, C.W.; Zoller, P. *Quantum Noise*, 2nd ed.; Springer: Berlin/Heidelberg, Germany, 2000.
49. He, B. Quantum optomechanics beyond linearization. *Phys. Rev. A* **2012**, *85*, 063820. [[CrossRef](#)]
50. Lin, Q.; He, B.; Ghobadi, R.; Simon, C. Fully quantum approach to optomechanical entanglement. *Phys. Rev. A* **2014**, *90*, 022309. [[CrossRef](#)]